 DOI: 10.1002/mats.200600012

Summary: The evolution dynamics of phase separation, coupled with shape deformation of vesicles is described by using dissipative dynamic equations, specifically the time-dependent Ginzburg-Landau (TDGL) equations. In order to improve the numerical stability and thus to efficiently deal with a large deformation of vesicles, a new algorithm, namely the discrete space variation model (DSVM) has been developed for the first time. The algorithm is based on the variation of the discretized free-energy functional, which is constructed in discrete membrane space, in contrast to the commonly used continuous free-energy functional. For the sake of numerical tractability, only the cylindrical vesicles (2D), with two components, are taken into consideration to illustrate the efficiency and validity of new algorithm. The simulation results, based on the DSVM algorithm have been compared with those from both linear analysis and strong segregation theory using the continuous space free-energy functional. It is found that the DSVM algorithm can correctly describe the coupling between the lateral phase-separation on the vesicle membrane and the vesicle shape deformation, both for early and late stages.

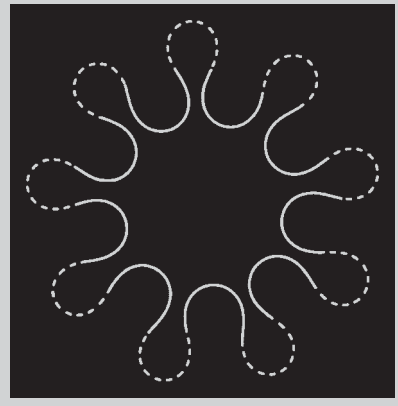

A flower-like vesicle obtained by DSVM simulation.

A Discrete, Space Variation Model for Studying the Kinetics of Shape Deformation of Vesicles Coupled with Phase Separation

*Jianfeng Li, Hongdong Zhang, Ping Tang, Feng Qiu, Yuliang Yang**

Key Lab of Molecular Engineering of Polymers, Ministry of Education of China and
Department of Macromolecular Science,
Fudan University, Shanghai 200433, China
Fax: +86-21-65643412; E-mail: ylyang@fudan.ac.cn

Received: January 23, 2006; Revised: March 9, 2006; Accepted: March 14, 2006; DOI: 10.1002/mats.200600012

Keywords: dynamics; phase separation; shape deformation; vesicles

Introduction

Amphiphilic molecules in aqueous solution often self-assemble as bilayer membranes that can form closed objects called *vesicles*. Using an elastic continuum model, the shapes of homogenous vesicles have successfully explained the shapes of real biomembranes, such as the biconcave shape of erythrocytes.[1] However, it is well known that real biomembranes are much more complex and multi-component systems. As a result, phase separation of the components can induce a complicated shape deformation.[2–6] Recently, it has also been found experimentally that, in a two-component system, the line tension of domain boundaries can cause a budding of the phase separated domains.[7]

In order to theoretically study the coupling between the phase separation and vesicle deformation, the deformation dynamics of two-component vesicles have been studied by the Monte-Carlo method[8,9] and a dramatic vesicle shape deformation has been observed during the evolution of the phase separation. However, the resulted vesicle shapes are rough due to the intrinsic fluctuations of the Monte Carlo algorithm. Phase-separation-induced vesicle shape transformation has also been studied by using the dissipative particle dynamics (DPD) method.[10–12] In the DPD model the amphiphilic molecules are modeled as a chain of beads to represent the polar head and hydrophobic tails, and thus the molecular mechanism of the phase-separation-induced shape transformation, such as budding, could be elucidated. The

 WILEY InterScience DISCOVER SOMETHING GREAT © 2006 WILEY-VCH Verlag GmbH & Co. KGaA, Weinheim

disadvantage of DPD is that the simulation system could not be too large, due to the limitation of computational resources. Another more effective simulation method for tackling this problem is based on the continuous-field model, and time-dependent Ginzburg-Landau (TDGL) dynamics.[13] By using this model, very impressive results were obtained, where the experimental observations on the shapes of the vesicle as well as the dynamic characteristics were reproduced. However, due to the adoption of the continuous elastic model for the membrane, the numerical discretization for a large local deformation, such as the phase-separated domains with very large local curvature, may cause serious numerical instability. More seriously, the phase domain boundaries on a deformable curved surface might be discontinuous, that is some singularities in the curvature could exist at the domain boundaries. Obviously, in this case, the continuous elastic model of the membrane will fail and thus it can only be applied in the case of small deformation and in the early stage of the phase separation.

In order to overcome this difficulty, we designed a new algorithm to simulate the phase-separation-induced vesicle deformation. As a first step, we considered a 2D membrane. A cross-section of a tubular vesicle can be viewed as a 2D simplification. Although, the results for the 2D model cannot exhibit the many interesting shapes of 3D vesicles,[7] a 2D confirmation of this algorithm is meaningful and 2D calculation provides mathematical clearance and transparencies. In the new algorithm, we first modeled the membrane (in the 2D case the membrane is simplified as a line) as an assembling of short bonds; their bending rigidity is assigned to the bond angles, θ. Afterwards, the Helfrich free-energy functional[13,14] is directly constructed on this spatially discretized membrane, referred to as the discrete space variation model (DSVM).[15] Obviously, the important difference from the continuous elastic free-energy model is that the discretization in our model is physical rather than numerical, and hence our model bears a large local curvature and numerical stability is improved. Finally, variation of this discretized free-energy functional, with respect to the discretized variables, was performed to obtain discrete kinetic equations directly. This model is free from the limitation of small spatial difference steps and numerical stability is ensured.

In this paper, the general description of the 2D DSVM is addressed in the section of *Model and Algorithm*. In the section of *Results and Discussion*, the early-stage behavior of the phase-separation-induced vesicle shape deformation is analyzed by using linearized stability analysis. Furthermore, the simulation results are presented and compared with the results obtained from strong segregation theory.[16] Some interesting results obtained by DSVM are presented to show how efficient and numerically stable this approach is.

Model and Algorithm

Similar to the model for the two-component vesicle by Taniguchi,[13] it was assumed that the membrane is locally incompressible and that the total amounts of amphiphiles A and B on the vesicle membrane are conserved during the evolution. In addition, the membrane's local bending modulus was determined by the local composition of the concentrations of the amphiphiles: ϕ_A and ϕ_B where $\phi_B = 1 - \phi_A$. For simplicity, a linear relationship was assumed, that is $\kappa = \kappa_A\phi_A + \kappa_B\phi_B = \kappa_0 + \zeta\phi$ where $\phi = \phi_A - \phi_B$, $\kappa_0 = (\kappa_A + \kappa_B)/2$ and $\zeta = (\kappa_A - \kappa_B)/2$. Similarly, the local spontaneous curvature is also composition dependent and can be simply expressed as $H_{sp}(\phi_A, \phi_B) = h_A\phi_A + h_B\phi_B = h_0 + \varepsilon\phi$ with the average spontaneous curvature given by $h_0 = (h_A + h_B)/2$ and the difference of the spontaneous curvatures between the two components given by $2\varepsilon = h_A - h_B$.

In our model, the membrane contour line is decomposed into N discrete, successively connected beads with position vectors $\mathbf{r}_k$ and bond vectors $\boldsymbol{\tau}_k = \mathbf{r}_k - \mathbf{r}_{k-1}$ ($k = 1, 2, 3, \ldots, N$), as schematically shown in Figure 1. To ensure the closure of the vesicle, we have the boundary condition of $\mathbf{r}_{N+1} = \mathbf{r}_0$. The composition of amphiphiles ϕ is assigned to the beads rather than the bonds connecting them.

With the model from Figure 1, the free-energy functional based upon discrete space can be written as:

$$F = \sum_{k=1}^{N} \frac{\kappa_0}{4}(H_k - \varepsilon\phi_k - h_0)^2(|\boldsymbol{\tau}_k| + |\boldsymbol{\tau}_{k+1}|) + \frac{P}{2}\sum_{k=1}^{N}\mathbf{r}_k\mathbf{n}_k|\boldsymbol{\tau}_k| + \sum_{k=1}^{N}\frac{b}{2}(\phi_k - \phi_{k-1})^2|\boldsymbol{\tau}_k| + \sum_{k=1}^{N} f(\phi_k)\frac{|\boldsymbol{\tau}_k| + |\boldsymbol{\tau}_{k+1}|}{2} \quad (1)$$

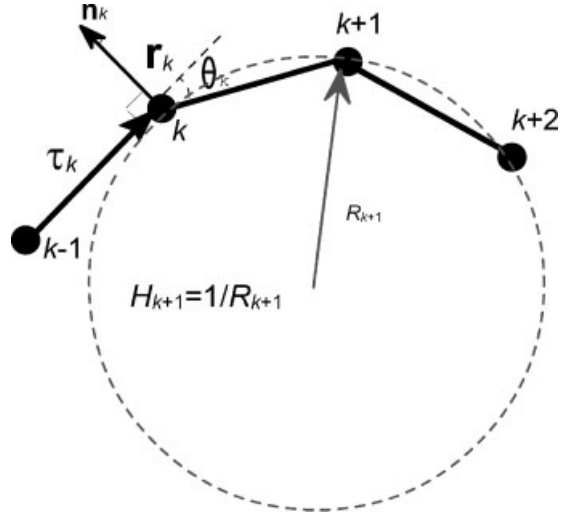

Figure 1. A discretized 2D vesicle composed of N beads with closed contour ($\mathbf{r}_{N+1} = \mathbf{r}_0$). The bond vector is $\boldsymbol{\tau}_k = \mathbf{r}_k - \mathbf{r}_{k-1}$ and $|\boldsymbol{\tau}_k|$ is the distance between the k^{th} and $(k-1)^{\text{th}}$ beads. $\mathbf{n}_k$ is the normal vector which is perpendicular to the bond vector $\boldsymbol{\tau}_k$. H_{k+1} is the local curvature of the $(k+1)^{\text{th}}$ beads which is defined as inverse to the radius: $H_{k+1} = \frac{2\sin\theta_{k+1}}{|\mathbf{r}_{k+2} - \mathbf{r}_k|}$.

 © 2006 WILEY-VCH Verlag GmbH & Co. KGaA, Weinheim

Here, the first term on the right hand side is the bending elastic energy, with the mean curvature being $H_k/2$ (see Figure 1) and $P = p_{out} - p_{in}$, representing the pressure difference across the vesicle. For simplicity, we have set $\zeta = (\kappa_A - \kappa_B)/2 = 0$, meaning that there is no bending modulus difference between the two components. The last two terms are related to the Ginzburg-Landau-DeGennes free energy.[17] The third term is the interface energy with the correlation length $b^{1/2}$. In the last term, $f(\phi_k) = -a_2\phi_k^2/2 + a_4\phi_k^4/4$, where a_2 and a_4 are phenomenological parameters and a_2 is related to the temperature, representing the quench depth. We note that if we set $\zeta = 0$ and the coupling constant $\Lambda = -\varepsilon\kappa_0$, we have $f(\phi_k) \to f(\phi_k) + h_0\Lambda\phi_k - \Lambda^2\phi_k^2/(2\kappa_0)$, and hence Equation (1) is reduced to the free-energy functional used by Taniguchi.[13] Therefore, it is clear that the phase-separation temperature has been lowered, i.e., $\tilde{a}_2 = a_2 + \frac{\Lambda^2}{\kappa_0}$, due to the coupling between the phase separation and vesicle deformation. Furthermore, the average spontaneous curvature h_0 only contributes a constant to the free energy[16] and thus omitted in the following.

Note that in Equation (1) there are two kinds of length elements: $|\boldsymbol{\tau}_k| = |\mathbf{r}_k - \mathbf{r}_{k-1}|$ and $(|\boldsymbol{\tau}_k| + |\boldsymbol{\tau}_{k+1}|)/2$, in relation to two beads and three beads, respectively. For example, for different values of $\frac{b}{2}(\phi_k - \phi_{k-1})^2$, between beads k and $k-1$, the distance between the two beads should be the length element $|\boldsymbol{\tau}_k| = |\mathbf{r}_k - \mathbf{r}_{k-1}|$. While, for the mixing free energy of the k^{th} bead, $f(\phi_k)$, the length element takes the average of the distances, $|\mathbf{r}_k - \mathbf{r}_{k-1}|$ and $|\mathbf{r}_{k+1} - \mathbf{r}_k|$ related to three beads $k-1$, k and $k+1$, i.e., $(|\mathbf{r}_k - \mathbf{r}_{k-1}| + |\mathbf{r}_{k+1} - \mathbf{r}_k|)/2 = (|\boldsymbol{\tau}_k| + |\boldsymbol{\tau}_{k+1}|)/2$ is employed to reasonably represent the average length element needed for $f(\phi_k)$ at the bead k. Furthermore the definition of the mean curvature is not the commonly used form, $H_k = 2\theta_k/|\mathbf{r}_{k+1} - \mathbf{r}_{k-1}|$, which is invalid for a large deformation. In discrete space, the mean curvature at bead k is given by the inverse of the radius of the circumcircle of the adjacent triangle: $H_k = 2\sin\theta_k/|\mathbf{r}_{k+1} - \mathbf{r}_{k-1}|$, as shown in Figure 1. Therefore, the free-energy functional of Equation (1) can be applied in the case of large deformation of the vesicle.

Following Taniguchi's idea,[13] the phase-separation-induced vesicle deformation can be solved using the simplest dissipative model, the time-dependent Ginzburg-Landau (TDGL) equations in the form of discrete space.

$$\frac{\partial \mathbf{r}_k}{\partial t} = -L_r \frac{\delta\left[F + \sum_{k=1}^{N}\gamma_k|\boldsymbol{\tau}_k|\right]}{\delta \mathbf{r}_k} = -L_r\{A_k\mathbf{n}_k + B_k|\boldsymbol{\tau}_k|\boldsymbol{\tau}_k\}\left(\frac{|\boldsymbol{\tau}_k| + |\boldsymbol{\tau}_{k+1}|}{2}\right)^{-1} \quad (2)$$

$$\frac{\partial \phi_k}{\partial t} = L_\phi \nabla^2\left[\frac{\delta F}{\delta \phi_k}\left(\frac{|\tau_k| + |\tau_{k+1}|}{2}\right)^{-1}\right] \quad (3)$$

where L_r and L_ϕ are two kinetic coefficients, γ_k is a local Lagrange multiplier which is introduced to guarantee the local incompressibility of the membrane, and the Laplace operator $\nabla_D^2 X_k = X_{k+1}\tau_{k+1}^{-2} + X_{k-1}\tau_k^{-2} - (\tau_k^{-2} + \tau_{k+1}^{-2})X_k$. A_k and B_k are normal and tangential forces, respectively, and are expressed as

$$\begin{aligned} A_k &= \sum_{i=-1,0,1}[D_i(k-i)G_{k-i}] + \frac{P}{2}(\cos\theta_k|\tau_{k+1}| + |\boldsymbol{\tau}_k|) \\ &\quad - \overline{\gamma}_{k+1}\sin\theta_k \\ B_k &= \sum_{i=-1,0,1}[E_i(k-i)G_{k-i}] - \frac{P}{2}\sin\theta_k|\boldsymbol{\tau}_{k+1}||\boldsymbol{\tau}_k| \\ &\quad - \overline{\gamma}_{k+1}\cos\theta_k|\boldsymbol{\tau}_k| \end{aligned} \quad (4)$$

where

$$\begin{aligned} \overline{\gamma}_k &= \gamma_k - b(\phi_k - \phi_{k-1})|\boldsymbol{\tau}_k|^{-1}/2 + [f(\phi_{k-1}) \\ &\quad + f(\phi_k)]/2 + \kappa_0[(H_k - \varepsilon\phi_k)^2 \\ &\quad + (H_{k-1} - \varepsilon\phi_{k-1})^2]/2 \end{aligned} \quad (5)$$

and $\overline{\gamma}(k)$ satisfies the relation

$$a\overline{\gamma}(k+1) + b\overline{\gamma}(k) + c\overline{\gamma}(k-1) = d \quad (6)$$

The expressions for a, b, c and d in the above equation, and $D_i(k)$, $E_i(k)$ and G_k in Equation (4) are given in the Appendix. Equation (6) is a tri-diagonal system, which can be easily solved.

Also we have:

$$\begin{aligned} \frac{\delta F}{\delta \phi_k} &= \kappa_0\varepsilon(\varepsilon\phi_k - H_k) + \frac{\partial f(\phi_k)}{\partial \phi_k} + 2b[\phi_k(|\boldsymbol{\tau}_k|^{-1} \\ &\quad + |\boldsymbol{\tau}_{k+1}|^{-1}) - \phi_{k-1}|\boldsymbol{\tau}_k|^{-1} \\ &\quad - \phi_{k+1}|\boldsymbol{\tau}_{k+1}|^{-1}](|\boldsymbol{\tau}_k| + |\boldsymbol{\tau}_{k+1}|)^{-1} \end{aligned} \quad (7)$$

The algorithm described above is referred to as the discrete space variation model (DSVM), as this model is based on the direct variation with respect to the free-energy functional, built on a spatially discrete membrane, to derive the discrete phase separation kinetics and deformation equations. When $N \to \infty$ and $|\boldsymbol{\tau}_k| \to 0$, the kinetic equations, Equation (2) and (3), obtained by DSVM reduced to those obtained by the continuous-field model derived by Taniguchi.[13] We should mention that the dissipative dynamic equations given in Equation (2) and (3) are not only the algorithm for searching for the minimum of the free-energy functional of Equation (1), but also describe the dynamics of the lateral phase separation on the membrane, coupled with the deformation of the vesicle shapes.

Results and Discussion

Comparison with Linear Analysis at the Initial Stage

In order to test the validity and accuracy of the simulation based on DSVM, we would first like to compare the

 © 2006 WILEY-VCH Verlag GmbH & Co. KGaA, Weinheim

simulation results with the linearized analysis of Equation (2) and (3), in the form of the continuous free-energy functional. In the following, we limit our treatment to the very beginning of the deformation coupled with phase separation. Following the linear analysis procedure of ref.[4] at the early stage of deformation the vesicle is assumed to be a circle with small and randomly distributed A and B components:

$$r(\theta) = r_0 + R(\theta)(\theta) \ll r_0$$
$$\phi(\theta) = \phi_0 + \Delta\phi(\theta)\Delta\phi(\theta) \ll 1 \quad (8)$$

$R(\theta)$ and $\phi(\theta)$ are then expanded into Fourier series:

$$R(\theta) = c_0 + \sum_{n=1}^{\infty} [c_n \cos n\theta + s_n \sin n\theta] \quad (9)$$

$$\phi(s(\theta)) = \phi_0 + \sum_{n=1}^{\infty} \left[\phi_{cn} \cos\frac{2\pi n}{L} s(\theta) + \phi_{sn} \sin\frac{2\pi n}{L} s(\theta)\right]$$
$$0 \le s \le L \quad (10)$$

where r_0 denotes the radius of the initial circle, and $\phi_0 = \frac{\int \phi ds}{L}$ is the average order parameter. By properly scaling the quantities as follows:

$$\tilde{p} \equiv \frac{Pr_0^3}{\kappa_0} \quad \bar{c}_n \equiv \frac{c_n}{r_0} \quad \tilde{\phi}_{cn} \equiv \frac{\Lambda r_0}{\kappa_0}\phi_{cn}$$
$$\bar{a}_2 \equiv \frac{\kappa_0(a_2 + \kappa_0\varepsilon^2 + \zeta\varepsilon h_0/2)}{\Lambda^2} \quad \tilde{b} \equiv \frac{\kappa_0 b}{\Lambda^2 r_0^2} \quad (11)$$

and only taking the cosine terms into consideration (the coefficients of the sine terms take the same form of the equations), the linearized equations are given by:

$$\frac{d\tilde{c}_n}{dt} = a(n)\tilde{c}_n + b(n)\,\widetilde{\phi}_{cn}$$
$$\frac{d\,\widetilde{\phi}_{cn}}{dt} = c(n)\tilde{c}_n + d(n)\,\widetilde{\phi}_{cn} \quad (12)$$

where $a(n) = -L_r\pi\kappa(n^2-1)(n^2-1-\tilde{p})/r_0^3$, $b(n) = -L_r\pi\kappa(n^2-1)/r_0^3$, $c(n) = -L_\phi\pi\Lambda^2(n^2-1)/r_0/\kappa$ and $d(n) = -L_\phi\pi\Lambda^2(\tilde{b}n^2 - \tilde{a}_2)/r_0/\kappa$.

Equation (12) also describes the dynamics at the very early stage of phase separation and the shape deformation and can be easily solved

$$\tilde{c}_n = A_1(n)e^{\rho_1(n)t} + A_2(n)e^{\rho_2(n)t}$$
$$\widetilde{\phi}_{cn} = B_1(n)e^{\rho_1(n)t} + B_2(n)e^{\rho_2(n)t} \quad (13)$$

with $A_1(n) = C_1/(\lambda_1 - \lambda_2)$, $A_2(n) = -C_2/(\lambda_1 - \lambda_2)$, $B_1(n) = C_1\lambda_2/(\lambda_1 - \lambda_2)$, and $B_2(n) = C_2(\lambda_1 - \lambda_2)/\lambda_1$. Where C_1 and C_2 are two integration constants. λ_1 and λ_2 are given

$$\lambda_{1,2} = \frac{a(n) - d(n) \pm \sqrt{(a(n) - d(n))^2 + 4b(n)c(n)}}{2b(n)}$$
$$(+\text{for } \lambda_1,\ -\ \text{for } \lambda_2) \quad (14)$$

The amplification factors $\rho_{1,2}$ are calculated by:

$$\rho_{1,2} = \lambda_{1,2}b(n) + d(n)b(n) \quad (15)$$

Obviously ρ_1 and ρ_2 ($\rho_{1,2}$) are both real and $\rho_1 > \rho_2$; thus in the very beginning ρ_1 will dominate the main growing mode. Solving the equation $d\rho_1(n)/dn = 0$, we obtain the fastest growing mode N_m, as well as the number of buds appearing in the vesicle contour.

Although it is not easy to directly calculate the amplification factors from Equation (2) and (3), the fastest growing mode at the very beginning of deformation can easily be obtained as described above, using linear analysis. Figure 2(a) shows the amplification factor (Equation (15)), which represents the rate of phase separation and shape deformation for the fastest growing mode versus the reduced quench depth denoted by a_2. Figure 2(b) shows the fastest growing mode versus the reduced quench depth

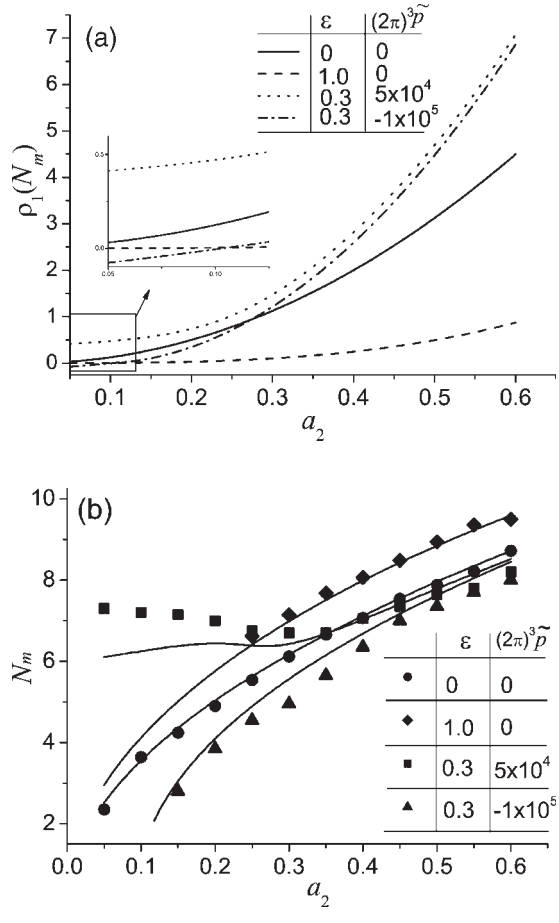

Figure 2. Comparison of results simulated using DSVM with results from linear analysis at the beginning of the evolution. (a) The plot of the amplification factors $\rho_1(N_m)$ versus a_2 by linear analysis (Equation (15)) where N_m is the fastest growing mode of $\rho_1(n)$; (b) The comparison between the fastest growing modes at the initial stage of the DSVM simulation (the symbols) and the results of the linear analysis (the solid lines). $\langle\phi_A\rangle = \langle\phi_B\rangle$, $L_r = 1.0$, $L_\phi = 1.0$, $L = 2\pi r_0 = 100$, $\kappa_0 = 1.0$, $\zeta = 0$. The inset shows the phase separation at small a_2.

 © 2006 WILEY-VCH Verlag GmbH & Co. KGaA, Weinheim

and is compared with results obtained from the linear analysis based on free-energy functional built in continuous space by Taniguchi et al.[4] It is seen from Figure 2(b) that, in general, the fastest growing mode N_m is increasing with an increase in the reduced quench depth. Accordingly, the rate of phase separation and shape deformation increase with an increase in the reduced quench depth, as shown in Figure 2(a). The pressure difference between the outer and inner sides of a vesicle, however, can seriously influence the behavior of the phase separation. When we increase the outer pressure to be $\tilde{p} = 5 \times 10^4/(8\pi^3)$, relative to the case of $\tilde{p} = 0$, the rate of phase separation will be accelerated, shown in Figure 2(a), and the domain size becomes small at lower a_2, shown in the inset of Figure 2(a). However, in Figure 2(b), when a_2 reaches 0.35, the phase domain size becomes slightly larger with an increase in the outer pressure, while the domain size decreases again following the general tendency when $a_2 > 0.35$. In contrast, when the inner pressure is higher, for example, $\tilde{p} = -1.0 \times 10^5/(8\pi^3)$, the rate of phase separation will be accelerated when $a_2 > 0.28$ but will decrease when $a_2 < 0.28$. However, the phase domain size increases with increasing a_2. From Figure 2(b) we conclude that our DSVM simulation results agree quite well with the linearized analysis based on the continuous free-energy functional and confirm the validity and accuracy of our DSVM algorithm.

It is seen from Figure 2(a) that the amplification factors for the fastest growing mode decrease when we increase

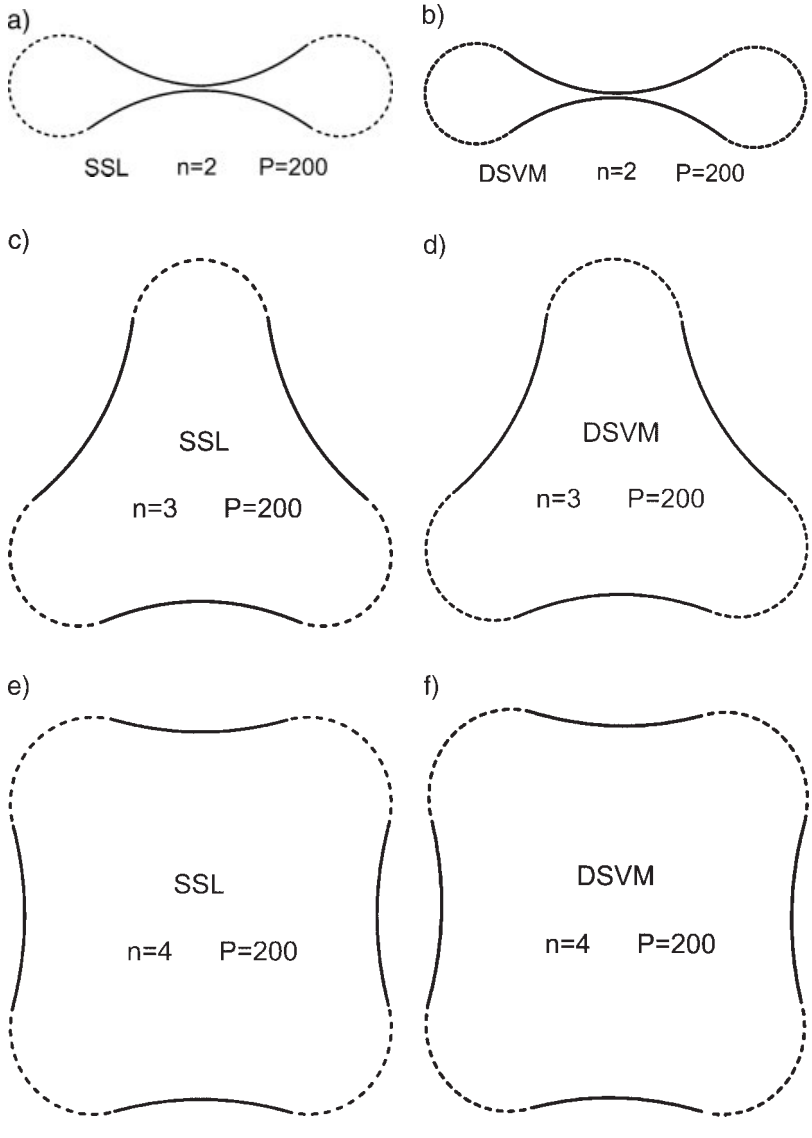

Figure 3. The comparison between resulting vesicle shapes, obtained by DSVM, and those from the strong segregation limit method for critical quench $\langle\phi_A\rangle = \langle\phi_B\rangle$. n denotes the modes of separation, P is the pressure and $\varepsilon/L = 10$ where L is the total length of the contour line. The solid and dotted lines represent the A and B components, respectively.

 © 2006 WILEY-VCH Verlag GmbH & Co. KGaA, Weinheim

$\varepsilon = \frac{h_A - h_B}{2}$. The effect of the pressure difference across the vesicle membrane is a bit complex. For the case of $\tilde{p} > 0$, the amplification factor for the fastest mode always has a positive value and is higher than that for $\tilde{p} = 0$. However, for the case of $\tilde{p} > 0$, the amplification factor for the fastest mode becomes negative when $a_2 < 0.12$, shown in the inset of Figure 2(a). Therefore, Figure 2(a) clearly demonstrates the coupling between phase separation and shape deformation of the vesicle: the critical temperature of phase separation can be raised or lowered depending on the parameters $\tilde{p}$ and ε controlling the vesicle shapes.

Comparison with Strong Segregation Theory at the Late Stage

The late stage solution of Equation (2) and (3) corresponds to finding the minimum in the free-energy functional of Equation (1). In order to ensure that the TDGL equations based on our model (DSVM) reaches the minimum for different folds of symmetry n, it is necessary to compare our DSVM simulation results to those obtained by strong segregation theory using the free-energy functional in continuous space proposed by Kawakatsu and coworkers.[16] In the strong segregation theory, an A/B mixture separates into A domains with composition $\phi_A = 1$ and B domains with $\phi_B = 1$, bounded by sharp domain walls. Once the number of the domain is fixed, free-energy equations for the vesicle only depend on the shape of the vesicle and thus can be easily constructed. By minimizing these free-energy equations, the shape equation is obtained and numerically solved by an iterative method to reach the equilibrium shape of the vesicle.[16]

Similar to the strong segregation theory in ref.[16] we assume that at the beginning, two components are separated into $2n$ equal segments dyed with the pure components A and B alternatively, and that their distributions do not evolve any more. Therefore, only the deformation is taken into consideration and thus the validity of Equation (2) is checked. Then, we only consider the deformation of the vesicle to obtain the equilibrium shape with a DSVM simulation and the results are compared with those obtained, based on the strong segregation theory.[16] In Figure 3, it is seen that, both qualitatively and quantitatively, the results obtained by strong segregation theory and DSVM simulation agree with each other very well. Therefore, we can give DSVM the ''license'' to simulate the coupling between phase separation and deformation of multi-component vesicles.

Efficiency and Validity for Large Deformations

In order to test how correct and efficient this model is in dealing with large deformation of vesicles, some typical results from DSVM calculations are presented in Figure 4. In Figure 4(a) and (b), the initial state is a round circle with A and B components randomly dyed along the contour

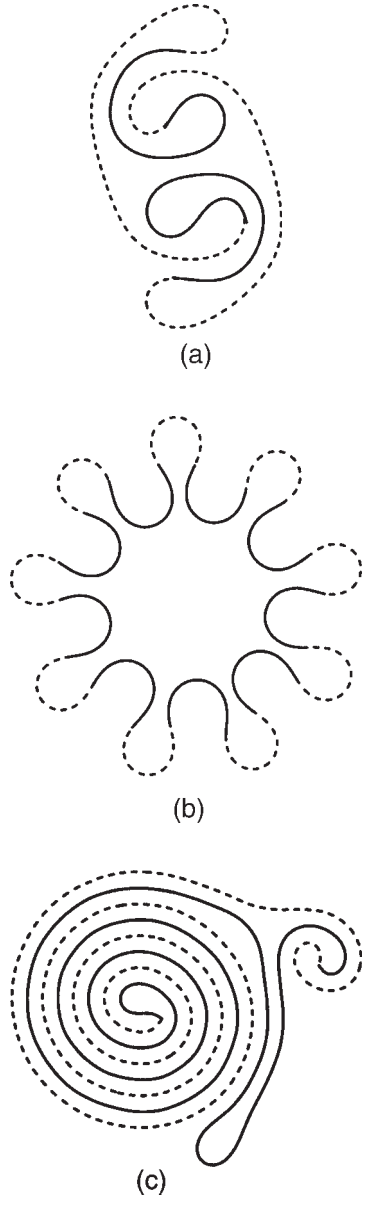

Figure 4. Vesicle deformation after 10 000 time steps. $r_0\varepsilon = 10$ where r_0 is the radius of the initial circle, $P = 0$, $\langle \phi_A \rangle = \langle \phi_B \rangle$, $a_2 = a_4 = 0.2$ and $|\tau_k| = 1.0$. The total length of the contour of the vesicle was: (a) $L = 100$ with 100 discrete points; (b) $L = 250$; and (c) $L = 400$. The solid and dotted lines represent the A and B components, respectively.

while in Figure 4(c) the initial state is two components separated into two equal segments which will not evolve further. Moreover, a long-range interaction is introduced into the total discrete free-energy functional, Equation (1), to avoid overlapping and crossing of the membrane.

During our simulation, it was found that the algorithm is numerically very stable. For example, we can simulate the dynamics of a vesicle composed of very small number of discrete points; see Figure 4(a). In fact, the membrane can

 © 2006 WILEY-VCH Verlag GmbH & Co. KGaA, Weinheim

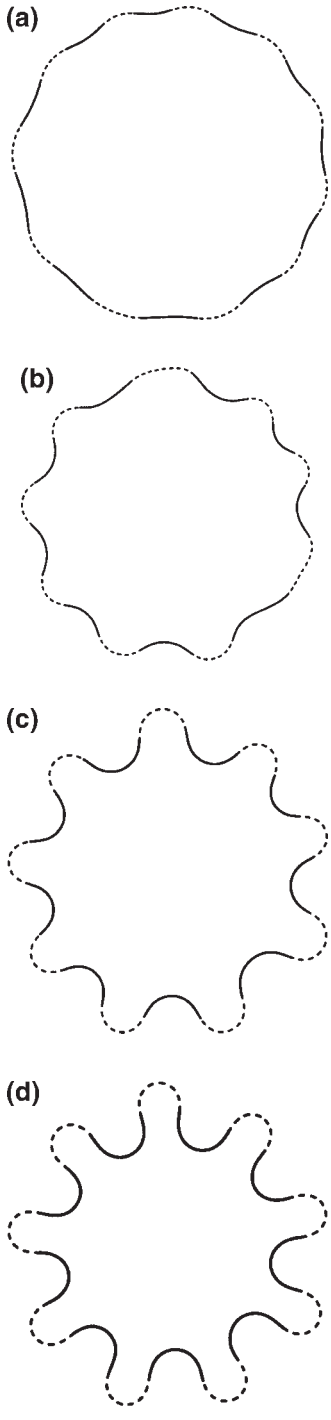

Figure 5. Dynamic evolution patterns of the vesicle shape, coupled with phase separation at different time steps (a) $t = 10^2$; (b) $t = 5 \times 10^2$; (c) $t = 2.5 \times 10^3$; (d) $t = 5 \times 10^3$; and (e) $t = 10^4$ (the same as in Figure 4(b), not shown here). The parameter settings are the same as in Figure 4(b).

be composed of fewer than 40 discrete segments. With this good numerical stability, DSVM is found to be valid for simulating large deformation of vesicles, shown in Figure 4(c). In addition to the numerical stability, the efficiency of the simulation is, at least, ten times higher than for the continuous free-energy functional model of the membrane. Furthermore, the results are very impressive and interesting, even though it is still a 2D model. The flower-like vesicle in Figure 4(b), whose evolution pictures at different time steps are shown in Figure 5 according to Equation (2) and (3), is very similar to the cross-section of one experimental result found in ref.[7] The vesicle shape of Figure 4(a) is a little like the shape of the inner membrane of mitochondria[18] and also Figure 4(c) is very interesting with a spiral shape that can be found very often in the biological systems.

Conclusion

Our DSVM model based on the variation of the discrete free-energy functional, directly built on the discrete membrane space has been developed to study the deformation of 2D vesicles coupled with phase separation. The results from linear analysis by Taniguchi[4] and strong segregation theory by Kawakatsu[16] have been used to check the accuracy and validity of the DSVM algorithm. It has been demonstrated that DSVM can correctly simulate the early stage, as well as the late stage behaviors of the shape deformation and phase separation of multi-component vesicles. In addition, DSVM is not only suitable in the case of large vesicle deformation, but also has high simulation efficiency. More importantly, it has also been demonstrated that DSVM is numerically very stable and the resulting shapes of vesicles are much more smooth than those by Monte-Carlo simulation. Finally, we should mention that, extending to the case of 3D vesicle is straight-forward, but a lengthy derivation and thus will be presented in the future publications.

Appendix

In Equation (4), the expressions of G_k, D_i and E_i, respectively, are as follows:

$$G_k = \frac{\partial[\kappa_0(H_k - \varepsilon\phi_k)^2/2]}{\partial H_k} = \kappa_0[H_k - \varepsilon\phi_k] \qquad \text{(A1)}$$

$$\begin{aligned} D_1(k) &= \frac{\cos\theta_k|\boldsymbol{\tau}_{k+1}|^{-1}}{|\mathbf{r}_{k+1} - \mathbf{r}_{k-1}|} - \frac{H_k(\mathbf{r}_{k+1} - \mathbf{r}_{k-1})\mathbf{n}_{k+1}}{|\mathbf{r}_{k+1} - \mathbf{r}_{k-1}|^2} \\ D_0(k) &= \frac{\sin^2\theta_k - 1 - \cos\theta_k|\boldsymbol{\tau}_{k+1}||\boldsymbol{\tau}_k|^{-1}}{|\boldsymbol{\tau}_{k+1}||\mathbf{r}_{k+1} - \mathbf{r}_{k-1}|} \\ D_{-1}(k) &= \frac{\sin\theta_{k-1}\sin\theta_k + \mathbf{n}_{k+1}\mathbf{n}_{k-1}}{|\boldsymbol{\tau}_k||\mathbf{r}_{k+1} - \mathbf{r}_{k-1}|} \\ &\quad + \frac{H_k(\mathbf{r}_{k+1} - \mathbf{r}_{k-1})\mathbf{n}_{k-1}}{|\mathbf{r}_{k+1} - \mathbf{r}_{k-1}|^2} \end{aligned} \qquad \text{(A2)}$$

 © 2006 WILEY-VCH Verlag GmbH & Co. KGaA, Weinheim

$$E_1(k) = -\frac{H_k(\mathbf{r}_{k+1} - \mathbf{r}_{k-1})\boldsymbol{\tau}_{k+1}}{|\mathbf{r}_{k+1} - \mathbf{r}_{k-1}|}$$
$$E_0(k) = \frac{\sin\theta_k \cos\theta_k |\boldsymbol{\tau}_k|}{|\boldsymbol{\tau}_{k+1}||\mathbf{r}_{k+1} - \mathbf{r}_{k-1}|}$$
$$E_{-1}(k) = \frac{[\sin\theta_k \cos\theta_{k-1} - \boldsymbol{\tau}_{k+1}\mathbf{n}_{k-1}|\boldsymbol{\tau}_{k+1}|]|\boldsymbol{\tau}_{k-1}|}{|\boldsymbol{\tau}_k||\mathbf{r}_{k+1} - \mathbf{r}_{k-1}|} + \frac{H_k(\mathbf{r}_{k+1} - \mathbf{r}_{k-1})\boldsymbol{\tau}_{k-1}}{|\mathbf{r}_{k+1} - \mathbf{r}_{k-1}|^2} \quad \text{(A3)}$$

The expression of coefficients in Equation (5) is given by

$$a = -\cos\theta_k(|\boldsymbol{\tau}_k| + |\boldsymbol{\tau}_{k+1}|)^{-1}$$
$$b = (|\boldsymbol{\tau}_k| + |\boldsymbol{\tau}_{k+1}|)^{-1} + (|\boldsymbol{\tau}_{k-1}| + |\boldsymbol{\tau}_k|)^{-1}$$
$$c = -\cos\theta_{k-1}(|\boldsymbol{\tau}_{k-1}| + |\boldsymbol{\tau}_k|)$$
$$d = \sin\theta_{k-1}[A_{k-1} + \overline{\gamma}_k \sin\theta_{k-1}](|\boldsymbol{\tau}_{k-1}| + |\boldsymbol{\tau}_k|)^{-1} - [|\boldsymbol{\tau}_k|B_k + \overline{\gamma}_{k+1}\cos\boldsymbol{\theta}_k](|\boldsymbol{\tau}_k| + |\boldsymbol{\tau}_{k+1}|)^{-1} + \cos\theta_{k-1}[|\boldsymbol{\tau}_{k-1}|B_{k-1} + \overline{\gamma}_k \cos\theta_{k-1}](|\boldsymbol{\tau}_{k-1}| + |\boldsymbol{\tau}_k|)^{-1} \quad \text{(A4)}$$

Acknowledgements: We thank the financial support from the *National Basic Research Program of China* (Grant No. 2005CB623800), the "Shuguang" Project of the *Shanghai Education Development Foundation*, the *National Special Fund for Excellent Ph.D. Dissertation of China* (Grant No. 200124) and for *Excellent Research Group of NSF of China*. The *NSF of China* (Grant Nos. 20474011, 20474012, 20374016 and 20104002) is also acknowledged.

[1] Z. C. Ou-Yang, W. Helfrich, *Phys. Rev. Lett.* **1987**, *59*, 2486.
[2] [2a] S. Leibler, *J. Phys. (Paris)* **1986**, *47*, 507; [2b] S. Leibler, D. Andelman, *J. Phys. (Paris)* **1987**, *48*, 2013.
[3] D. Andelman, T. Kawakatsu, K. Kawasaki, *Europhys. Lett.* **1992**, *19*, 57.
[4] T. Taniguchi, K. Kawasaki, D. Andelman, T. Kawakatsu, *J. Phys. II* **1994**, *4*, 1333.
[5] U. Seifert, *Phys. Rev. Lett.* **1993**, *70*, 1335.
[6] [6a] R. Lipowsky, *J. Phys. II* **1992**, *2*, 1825; [6b] F. Julicher, R. Lipowsky, *Phys. Rev. Lett.* **1993**, *70*, 2964.
[7] T. Baumgart, S. T. Hess, W. W. Webb, *Nature* **2003**, *425*, 821.
[8] R. Morikawa, Y. Saito, *J. Phys. Soc. Jpn.* **1995**, *64*, 3562.
[9] P. B. S. Kumar, G. Gompper, R. Lipowsky, *Phys. Rev. Lett.* **2001**, *86*, 3911.
[10] S. Yamamoto, Y. Maruyama, S. A. Hyodo, *J. Chem. Phys.* **2002**, *116*, 5482.
[11] M. Laradij, P. B. S. Kumar, *Phys. Rev. Lett.* **2004**, *93*, 198105.
[12] J. C. Shillcock, R. Lipowsky, *J. Chem. Phys.* **2002**, *117*, 5048.
[13] T. Taniguchi, *Phys. Rev. Lett.* **1996**, *76*, 4444.
[14] W. Helfrich, *Z. Naturforsch.* **1978**, *33a*, 305.
[15] J. F. Li, H. D. Zhang, F. Qiu, Y. L. Yang, *Acta. Phys. Sin. (in Chinese)* **2005**, *54*, 4000.
[16] T. Kawakatsu, D. Andelman, K. Kawasaki, T. Taniguchi, *J. Phys. II* **1993**, *3*, 971.
[17] J. W. Cahn, J. E. Hilliard, *J. Chem. Phys.* **1959**, *31*, 688.
[18] G. C. Karp, "*Cell and Molecular Biology*", John Wiley & Sons, New York 2002.

 © 2006 WILEY-VCH Verlag GmbH & Co. KGaA, Weinheim